

KINDLING THE FIRST STARS II: DEPENDENCE OF THE PREDICTED PISN RATE ON THE POP III INITIAL MASS FUNCTION

ALESSA IBRAHIM WIGGINS¹, MIA SAUDA BOVILL², LOUIS-GREGORY STROLGER³, MASSIMO STIAVELLI³, AND CORA BOWLING¹

¹Department of Physics and Astronomy, Texas Christian University, Fort Worth, TX

²Department of Astronomy, University of Maryland, College Park, College Park, MD and

³Space Telescope Science Institute, Baltimore, MD

Version February 28, 2024

ABSTRACT

Population III (Pop III) stars formed out of metal free gas in minihalos at $z > 20$. While their ignition ended the Dark Ages and begin enrichment of the IGM, their mass distribution remains unconstrained. To date, no confirmed Pop III star has been observed and their direct detection is beyond the reach of the James Webb Space Telescope (JWST) without gravitational lensing. However, a subset of massive Pop III stars end their lives in pair instability supernova (PISN). With typical energies of $\sim 10^{53}$ erg, PISN light curve peaks are bright enough to be detectable by JWST and the Roman Space Telescope. The fundamental question of this work is whether or not observed PISN can be used as a diagnostic of the Pop III IMF. In this work, we use a model of the formation of the first stars to determine the dependence of PISN rates at $z > 5$ for a range of Pop III power law IMFs ($\alpha = 0.2 - 2.35$) and, critically, the method by which the IMF is populated. At $z > 15$, we predict typical rates of $10^{-2} - 10^2$ per deg² per year which will produce $10^{-3} - 0.1$ /year in a single NIRC₂ pointing and $0.003 - 30$ /year in a single Roman pointing with $0.1 - 1000$ per year detected in the HLTDS. Our work highlights that theoretical modeling of PISN rates is required if upcoming PISN studies with JWST and Roman are going to constrain the Pop III IMF.

1. INTRODUCTION

Population III (Pop III) stars are a theoretical population of metal-free stars. It is normally assumed that they formed in dark matter minihalos with masses of $10^5 - 10^6 M_{\odot}$ at $z > 30$ (Abel et al. 2002). Their ignition ended the Cosmic Dark Ages, and their supernovae explosions enriched the interstellar and intergalactic mediums (Jaacks et al. 2018). However, to date, no confirmed Pop III star or star cluster has been observed, and without gravitational lensing, those at high- z remain beyond the reach of JWST (Gardner et al. 2006; Bovill et al. 2024).

Due to the inefficiency of the cooling of molecular hydrogen, Pop III stars are thought to be more massive than enriched Pop II and Pop I stars. Although it is widely agreed that typical Pop III stars are more massive compared to their enriched Pop II or Pop I counterparts, the precise mass distribution of Pop III stars remains uncertain. Certain investigations propose initial mass function upper limits reaching $1000 M_{\odot}$ or even higher (Bromm et al. 1999; Abel et al. 2000; Ohkubo et al. 2009). Conversely, other theoretical studies propose that Population III stars could exhibit a broad range of masses, potentially extending down to a solar mass or below (Stacy et al. 2016; Prole et al. 2022; Latif et al. 2022; Wollenberg et al. 2020; Sugimura et al. 2020; Clark et al. 2011; Greif et al. 2011; Susa 2013; Yoshida et al. 2006; Park et al. 2021a,b). Consequently, our understanding of both the shape of the Pop III stellar initial mass function (IMF) and the maximum mass for a Pop III star remain elusive. While their formation and evolution are likely distinct from that of enriched stars in the local Universe, they remain observationally unconstrained.

Directly detecting Pop III stars or Pop III star clusters at high- z is challenging as their magnitudes are too faint for even the deepest JWST observations (Rydberg et al. 2013; Bovill et al. 2024). Nevertheless, utilizing gravitational lensing shows promise, and has been studied with a focus on magnification in known lensing clusters (Zackrisson et al. 2015; Windhorst et al. 2018). Detecting Pop III stars through gravitational lensing necessitates accurate lensing models, which are available for various lensing clusters (Lam et al. 2014; Diego et al. 2016, 2015; Jauzac et al. 2015a,b). Additionally, individual stars magnified up to 10,000 times have been observed in caustics (Vanzella et al. 2020; Welch et al. 2022), providing evidence that these high-redshift stars could have masses exceeding $> 50 M_{\odot}$ (Welch et al. 2022). The volume probed by very high magnification lensing clusters is modest, which may make the direct observation of a Population III star unlikely.

Consequently, one of the most favorable methods to detect the earliest stars is indirectly through their supernovae. Specifically, a subgroup of Pop III stars with masses ranging from $140 - 260 M_{\odot}$ undergo what is known as a pair instability supernova (PISN) (Fowler & Hoyle 1964; Barkat et al. 1967; Rakavy et al. 1967). These explosive events release energy, perhaps exceeding 10^{53} erg, making them more than a hundred times more energetic than a typical core collapse supernova, although see Schulze et al. (2023) and Gal-Yam et al. (2009) for a highly likely candidates

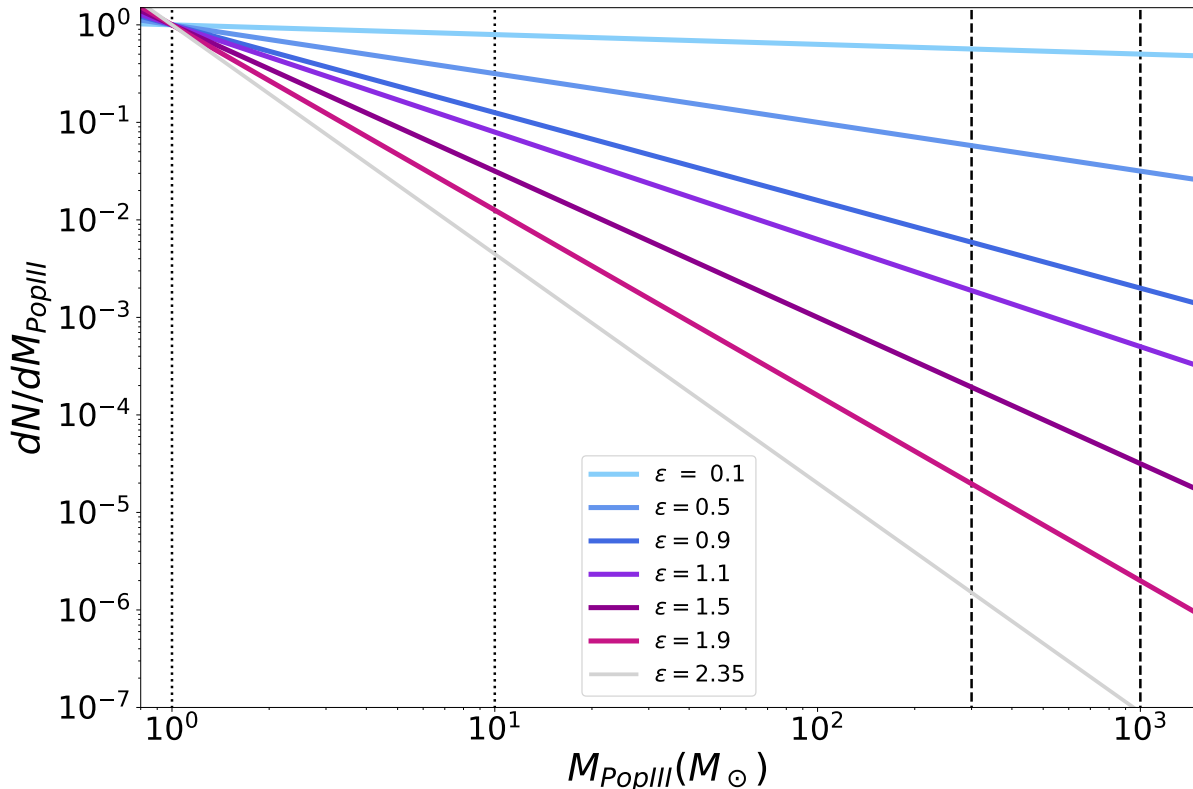


FIG. 1.— The range of slopes for the Pop III IMF considered in this work. The color coding in this figure will be used throughout this work for the various IMF slopes. The dotted vertical lines show the minimum Pop III masses considered in this work ($1 M_{\odot}$ and $10 M_{\odot}$) and the vertical dashed lines show the maximum Pop III masses considered in this work ($300 M_{\odot}$ and $1000 M_{\odot}$). This figure is analogous to Figure 2 in Bovill et al. (2024).

with lower energy. As a result, their peak luminosities are significantly high, enabling the possibility of mass detection using both the JWST and the Roman Space Telescope (Whalen et al. 2013; Wang et al. 2017; Moriya et al. 2022; Venditti et al. 2024). This is especially true for the expected depth ($\sim 28 - 29$ mag) and coverage ($5 - 12 \text{ deg}^2$) of the Roman High Latitude Time Domain Survey (Rose et al. 2021).

In addition to the unconstrained probability of a Pop III star forming in the PISN range, additional uncertainties need to be incorporated into the interpretation of observed PISN rates. Thus theoretical modeling, specifically that which can explore a multidimensional parameter space, is a critical component of any PISN survey. Currently, PISN rates have been modeled for a range of Pop III IMFs (Lazar & Bromm 2022; Briel et al. 2022; Venditti et al. 2024).

In this work, we present predictions for the intrinsic PISN rates for various Pop III IMFs using a range of methods to populate the IMF. We also introduce a Monte Carlo method for stochastically populating the Pop III IMF to account for the limited fragmentation of primordial gas (Stiavelli 2009; Bovill et al. 2024). In Section 2, we describe the simulations and the relevant components of our model and the calculation of the PISN rates. In Section 3, we present our predictions for the dependence of PISN rates on the Pop III IMF. Finally, we discuss our conclusions in Section 4.

2. SIMULATIONS AND MODELS

To calculate PISN rates in a cosmological volume we build a set of merger trees using the N-body simulations described in Bovill et al. (2024) with a comoving boxsize of $2 \text{ Mpc}/h$ on a side run from $z = 150$ to $z = 6$ with $N = 512$ and a dark matter particle of $\sim 10^3 M_{\odot}$. We assume a WMAP9 cosmology ($\Omega_M = 0.279$, $\Omega_{\Lambda} = 0.721$, $h_o = 0.7$) (Bennett et al. 2013). At our redshifts of interest ($z \sim 20 - 6$), the physical size of our box is $\approx 200 \text{ kpc}$ on a side. We robustly resolve halos with $M > 10^5 M_{\odot}$, including all potential sites of Pop III star formation. In addition, the positional information for each halo allows us to track external metal enrichment by supernova ejecta from nearby halos. Simulations were run with Gadget 2 (Springel 2005) on initial conditions generated by MUSIC (Hahn & Abel 2011) and analyzed with Amiga (Knollmann & Knebe 2009; Gill et al. 2004) and consistent trees (Behroozi et al. 2013).

Baryonic properties are added using the model described in Bovill et al. (2024) which models the Pop III star formation in a cosmological context. The model assumes Pop III stars only form in halos which are pristine, having not been enriched internally by previous episodes of star formation, nor externally by supernova ejecta from nearby halos.

Only Pop III stars in the model can produce PISN. We assume the Pop III stars form with an IMF which is a power-law $dN/dM = AM^{-\alpha}$ with a given Pop III minimum mass (m_{min}) and maximum mass (m_{max}). Due to the uncertainty in the slope of the Pop III IMF, we explore a range of slopes, with $\alpha = [0.1, 0.5, 0.9, 1.1, 1.5, 1.9, 2.1, 2.35]$, as shown in Figure 1. The most bottom heavy slope of $\alpha = 2.35$ corresponds to the Salpeter IMF for Pop I stars (Salpeter 1955). The evolution of the cosmic star formation history for the redshift range considered here is automatically included in the Bovill et al. (2024) model.

2.1. Calculating N_{PISN}

Before we can determine the rate of PISN, we first need to determine the number of stars which form in the PISN mass range ($140 - 260 M_{\odot}$) in a specific halo for a given Pop III IMF. To do this, we populate the Pop III IMF in three different ways, through mass normalization, number normalization, and through monte carlo population. For all three, we assume that every star which forms in the PISN mass range explodes as a PISN with an energy of 10^{53} erg.

2.1.1. Mass Normalization

The first method we use to populate the Pop III IMF is the one commonly used to calculate PISN rates for various potential Pop III IMFs (Lazar & Bromm 2022; Briel et al. 2022; Venditti et al. 2024). The number of PISN is determined by the integral of dN/dm for $140 M_{\odot} \leq m \leq 260 M_{\odot}$. In this first option the IMF is normalized by the maximum possible mass in Pop III stars, M_{III}^{max} ,

$$M_{\text{III}}^{max} = \epsilon_{\text{III}} f_b M_{vir} = \int_{m_{min}^{\text{III}}}^{m_{max}^{\text{III}}} A_M m^{\alpha+1} dm, \quad (1)$$

where M_{vir} is the virial mass of the halo, f_b is the cosmic baryon fraction, ϵ_{III} is the star formation efficiency of Pop III stars, and m_{max}^{III} and m_{min}^{III} are the maximum and minimum possible Pop III masses respectively. We use $\epsilon_{\text{III}} = 0.01$ which is the fiducial value used in Bovill et al. (2024). For the power law IMF assumed in this work, a halo with M_{vir} gives us a N_{PISN} of

$$N_{\text{PISN}} = \int_{140 M_{\odot}}^{260 M_{\odot}} A_M m^{\alpha} dm, \quad (2)$$

where A_M is the constant for a mass normalization of the Pop III IMF. When the Pop III IMF is populated this way two halos with the same M_{vir} will always have the same N_{PISN} . In addition, N_{PISN} is the sum of the probabilities of a star forming between $140 - 260 M_{\odot}$. Critically, this allows for a non-integer N_{PISN} , including one which is less than one.

2.1.2. Number Normalization

For this method, we use the assumption from Bovill et al. (2024) that inefficient cooling means primordial gas will not fragment as effectively as enriched gas, limiting the total number of fragments out of which Pop III stars can form. This places a limit on the *number* of Pop III stars which can form in a given halo.

Jeans collapse allows us to estimate the maximum number of fragments in a halo with M_{vir} at a given redshift, z , assuming an initial gas temperature of T_{vir} cooling to a final temperatures, T_f . If the gravitational collapse timescale, τ_{coll} , is less than the cooling time scale, τ_{cool} in the halo, the gas will collapse into a single fragment. However, for Pop III forming halos with $M \gtrsim 10^6 M_{\odot} ((1+z)/31)^{-2.07}$, the collapse timescale is longer than the cooling timescale. Therefore, the gas cools faster than it collapses, resulting in additional fragmentation (Bovill et al. 2024; Stiavelli 2009). Note, in this work, we are not accounting for more complex physics such as increases in fragmentation with the angular momentum of the halo, however, our simple model is able to reproduce the Pop III star formation efficiencies from Skinner & Wise (2020) (Bovill et al. 2024).

The maximum number of fragments, N_{frag} which can form from the primordial gas in a halo is given by

$$N_{frag} \leq 9.12 \left(\frac{M_{vir}}{10^6 M_{\odot}} \right)^{4/3} \left(\frac{1+z}{31} \right)^2 = \int_{m_{min}^{\text{III}}}^{m_{max}^{\text{III}}} A_N m^{\alpha} \quad (3)$$

where M_{vir} is the virial mass of the halo and z is the redshift of the halo. For the power law IMF assumed in this work, a halo with M_{vir} at z gives us a N_{PISN} of

$$N_{\text{PISN}} = \int_{140 M_{\odot}}^{260 M_{\odot}} A_N m^{\alpha} dm \quad (4)$$

where A_N is the normalization constant for normalization by number. As with § 2.1.1, when the Pop III IMF is populated this way two halos with the same M_{vir} at the same z will always have the same N_{PISN} . Once again, N_{PISN} is the sum of the probabilities of a star forming between $140 - 260 M_{\odot}$ allowing for a non-integer N_{PISN} , including values which are less than one.

2.1.3. Monte Carlo Population of the IMF

Our final method of populating the Pop III IMF is to use a Monte Carlo approach to populate the number of stars in the IMF. This method is more realistic for several reasons. First, the specific number and masses of stars at the high mass of the IMF is dominated by Poisson noise. Specifically, for low number statistics dominated by poisson noise, a large number of small probabilities summing to provide certainty of an event may not be an accurate model for the formation of massive stars. In addition, the statistical approach to populating the IMF assumes it is possible to have a have a fraction of a PISN *and* that when you add up all of those fractions, they add constructively.

The method we use to populate the IMF using a Monte Carlo technique is the same used in Bovill et al. (2024) and we describe it below.

1. First, we randomly populate a given Pop III IMF with a million stars of masses, m_{III}^i . As in § 2.1.1 and § 2.1.2, the IMF is defined by the slope of a power law and the minimum and maximum masses of the Pop III stars.
2. We then calculate the cumulative sum of the 10^6 Pop III ‘stars’ where $M_{III}^j = \sum_{i<j} m_{III}^i$ and truncate the number of ‘stars’ when $M_{III}^j < M_{III}^{max}$ where M_{III}^{max} is the maximum mass in Pop III stars which can be formed in a halo of a given M_{vir} .
3. Finally, we account for the limited fragmentation of primordial gas by truncating stars a second time so that the total number of Pop III stars, $N_{III} < 6N_{frag}$, where N_{frag} is the integer value of the maximum number of fragments in a primordial gas for a halo with a given M_{vir} and z (Equation 3), and 6 is the maximum number of Pop III stars which form per fragment (Susa et al. 2014).

The number of PISN is determined by how many of the remaining stars are between $140 M_{\odot}$ and $260 M_{\odot}$. Unlike when the IMF is populated statistically, this will always be an integer number and be different each time the IMF of a halo is populated with a different initial set of ‘stars.’

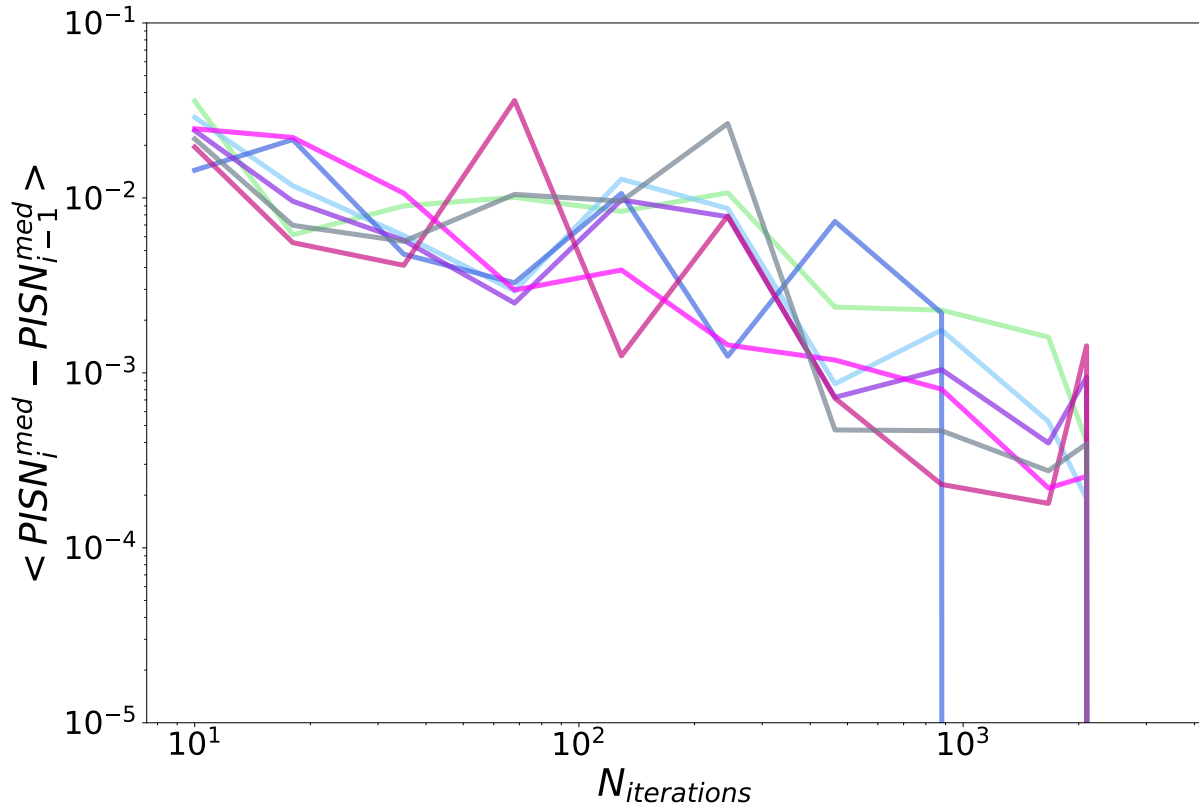


FIG. 2.— Mean of the difference between the median of the N_{PISN} per halo versus, N , the number of times we use our Monte Carlo method to populate the IMF for $N = (10, 18, 35, 68, 129, 244, 464, 879, 1668, 3162)$. This shows that for $N = 1000$ we are convergent to within 10^{-3} , which is two order of magnitude below the difference in PISN rates of similar Pop III IMFs.

We populate the IMF N times and determine the median and standard deviation of N_{PISN} in each halo. For a specific Pop III IMF, the median N_{PISN} is considered the typical N_{PISN} for a given halo and the standard deviation

measures the inherent scatter in N_{PISN} for a given halo. The latter is critical for the interpretation of PISN rates as it quantifies whether there is an *observable* difference in the PISN rate for various Pop III mass distributions.

We choose 1000 iteration of the Monte Carlo method because it provides convergence which is an order of magnitude less than the inherent scatter in the number of PISN for a given Pop III IMF. In Figure 2, we demonstrate this by plotting the average difference in the median PISN for 10 - 3000 iterations. For $N_{\text{iter}} \geq 1000$ iterations the change in the median PISN rate would not produce any meaningful change in our predictions.

2.2. PISN Rate Calculation

In this section, we describe how we converted the number of PISN per halo in our models into predictions for the observed PISN rate per square degrees (Figure 3). After populating the Pop III IMF, we first determine the total number of PISN in each halo for every snapshot in the N-body simulation. Second, we smooth this in redshift using a kernel with $\Delta z = 0.5$, where our chosen Δz is determined by the typical band width of the NIRCcam wide filters on JWST for emission in the rest frame UV (Rieke et al. 2008).

The next step is to calculate the number density of PISN at a given z per square degree by dividing the smoothed number of PISN by the angular size of the simulation box at that redshift. The penultimate step is to transform the number density of PISN on the sky at a given redshift to a PISN *rate* per square degree. We then divide the number density of PISN at each redshift by the time between simulation outputs (10 Myr). Finally, we add the effects of time dilation due to the expansion of spacetime by multiplying the PISN rates by $(1 + z)$ (Weinmann & Lilly 2005).

3. RESULTS

The fundamental question of this work is whether or not observed PISN can be used as a diagnostic of the Pop III IMF. The short answer to this question is yes, however there are important caveats.

Calculating a PISN rate from an underlying population of Pop III stars requires assumptions about how the high mass end of that IMF is populated. Therefore, how the PISN rates detected by JWST and Roman can be interpreted depends on what assumptions the models make.

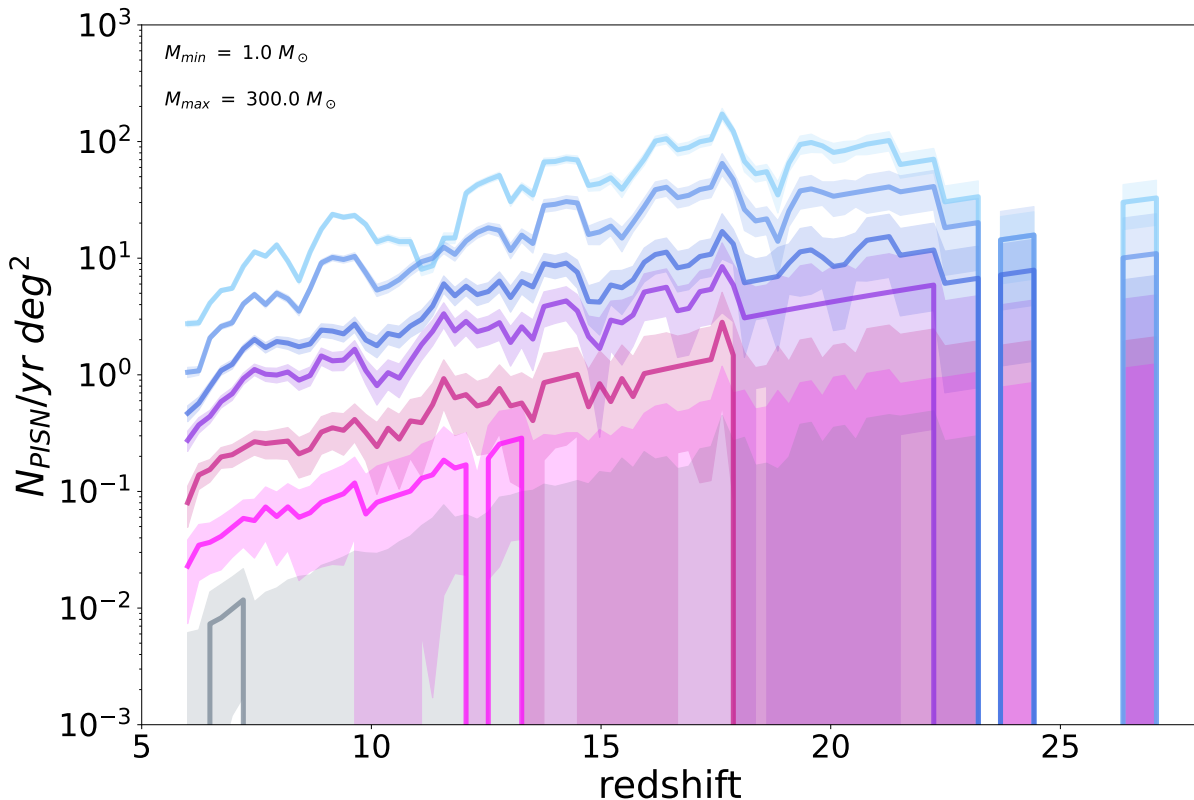


FIG. 3.— The PISN rates calculated using a Monte Carlo population of the Pop III IMF for $m_{\text{min}}^{\text{III}} = 1.0 M_{\odot}$ and $m_{\text{max}}^{\text{III}} = 300 M_{\odot}$. Solid lines show the median PISN rate for 1000 iterations of the IMF population, and the shaded region show the expected range of PISN rates for each IMFs. The colors correspond to the IMF slopes in Figure 1.

We begin with the PISN rates calculated from Pop III IMFs populated with the Monte Carlo method described in § 2.1.3. The median PISN rates in Figure 3 show a spread of 4 - 5 orders of magnitude for $\alpha = 2.35 - 0.1$.

However, when the Pop III IMF is populated using our Monte Carlo approach, a halo with a given M_{vir} at a given redshift, z , will not always have the same N_{PISN} . This produces an inherent scatter in the PISN rate for a given Pop III IMF, quantified by the standard deviation in the PISN rate and shown as the shaded regions in Figure 3. Critically, in order for observed PISN rate to be an effective tool to constrain the Pop III IMF, the difference between PISN rates for different Pop III IMFs must be *greater* than the inherent scatter in the PISN rate for each IMF. This is illustrated by the comparisons between the bottom heavy ($\alpha = (2.35, 2.1, 1.9)$) and top heavy ($\alpha = 1.5 - 0.1$) IMFs in Figure 3.

For all IMFs considered in this work, the difference in the median modeled PISN rates is large enough to allow PISN rates observed by JWST and Roman to provide significant constraints. When the inherent scatter for a given IMF is taken into account the picture is more complex.

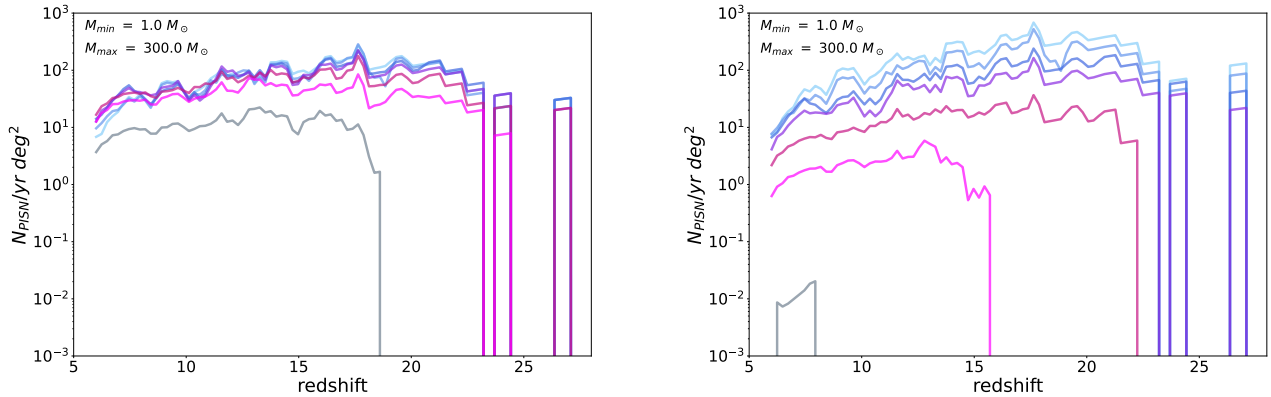


FIG. 4.— (Left) The PISN rates for the Pop III initial mass functions show in Figure 1 assuming the Pop III IMF is normalized by mass. (Right) PISN rates for the Pop III initial mass functions show in Figure 1 assuming the Pop III IMF is normalized by number.

For the top heavy IMFs the inherent scatter is smaller than the differences between the median PISN rates. Therefore the PISN rate can be used to differentiate between various top heavy IMFs at $z < 15$. For bottom heavy IMFs the inherent scatter is *larger* than the differences in the PISN rates except for $z < 9 - 10$. Thus, observed PISN rate will be of only limited use when differentiating between bottom heavy Pop III IMFs. In addition, at $z > 15$, the inherent scatter is greater than the differences for all IMFs considered in this work, severely limiting the efficacy of observed PISN rates as a constraint on the Pop III IMF.

We next quantify how our Monte Carlo method of populating the IMF changes the predicted PISN rates compared to the statistical method used in other work. Figure 4 shows the PISN rates calculated from a statistical population of a Pop III IMF normalized by the total mass of Pop III stars and the number of Pop III stars as described in § 2.1.1 and § 2.1.2.

When the IMF is statistically populated, and normalized by mass, we find PISN rates of $10^1 - 10^2$ per square degree per year with minimal dependence of the PISN rate on the Pop III IMFs for the IMFs probed in this work

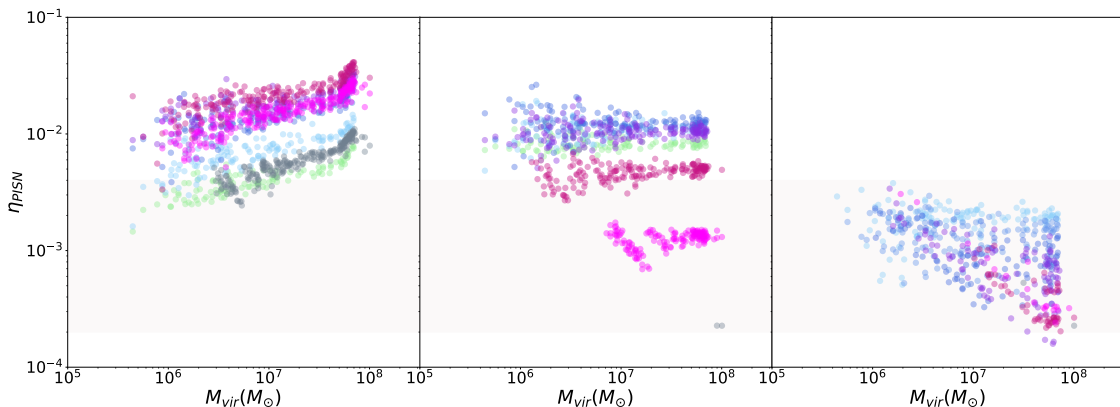


FIG. 5.— The efficiency of PISN formation for the three methods we use to populate the Pop III IMF, normalized by mass (left), normalized by number (center), and using our Monte Carlo approach (right). The colors of the points correspond to the Pop III IMFs shown in Figure 1 and the shaded region shows the PISN efficiency range given in Lazar & Bromm (2022).

As seen in Figure 5, we find that our results are in broad agreement with Lazar & Bromm (2022). For our mass normalized models, our slightly higher values are likely due to the lack of an exponential cut off in our Pop III IMFs.

However, for all three methods, we produce PISN efficiencies, $\epsilon_{\text{PISN}} = N_{\text{PISN}}/M_{\text{III}}$, which are in agreement with the range reported in their work. This implies that for similar Pop III IMFs, ϵ_{PISN} is roughly convergent for different methods of calculating the PISN rate.

When the IMF is statistically populated and normalized by the maximum number of Pop III stars (Equation 3), we find a stronger dependence of the modeled PISN rates on the Pop III IMF, with a spread of 2 – 3 orders of magnitude in the PISN rates for the IMFs probed in this work. In addition, we see a stronger evolution with redshift, which is expected given the $(1 + z)^{4/3}$ dependence on the number of Pop III star forming fragments in primordial gas.

Note, for both normalizations, populating the Pop III IMFs statistically produces roughly an order of magnitude higher PISN rates than the Monte Carlo population of the IMF.

It is critical to remember that when we observe a PISN rate all we will know is how many PISN have gone off in a year in a given square degree of the sky in a given redshift range. Comparisons between Figures 3 and 4 demonstrate how important it is to consider how the IMF is populated before interpreting the observational PISN rates. To illustrate this we will consider a detection of approximately 1.0 PISN per year at $z = 10$ assuming a Pop III stellar mass range of $1.0 - 300 M_{\odot}$.

For the mass normalized IMFs, this PISN rate is not consistent with any of the IMFs considered in this work. In fact, it is lower than that expected for even the most bottom heavy IMFs. One potential interpretation of this result is that only a fraction of Pop III stars between $140 M_{\odot}$ and $260 M_{\odot}$ explode in a PISN (Heger et al. 2003; Heger & Woosley 2010). For Pop III IMF normalized to the fragmentation of the primordial gas, this PISN rate would suggest a bottom heavy IMF equivalent to a power law with $\alpha = 1.9$. Finally, when the IMF is populated using a Monte Carlo approach the same PISN rate would suggest a moderately top heavy IMF with $\alpha \approx 1.0$.

4. DISCUSSION AND CONCLUSIONS

Roman and JWST are the first telescopes with the potential to detect PISN (Whalen et al. 2013; Wang et al. 2017; Moriya et al. 2022; Venditti et al. 2024). In this work, we produced predictions for PISN rates for a range of Pop III IMFs and three methods for populating the Pop III IMF. The result presented in this work highlight the critical roll theoretical modeling must play in the extraction of the astrophysics of the underlying stellar populations from the observed PISN rates.

- Depending on the Pop III mass distribution and the method by which we populate the IMF, we predict $10^{-2} - 10^2$ PISN per square degree per year. This would produce $10^{-3} - 0.1/\text{year}$ in a single NIRCcam pointing and $0.003 - 30/\text{year}$ in a single Roman pointing with $0.1 - 1000$ per year detected in the HLTDS. In particular, for top heavy IMFs, this almost guarantees detection of a PISN with Roman’s HLTDS, assuming all Pop III stars with $140 < m < 260 M_{\odot}$ explode as a PISN.
- When done in concert with the modeling of PISN rates for a given Pop III IMF, PISN rates observed with JWST and Roman will be able to differentiate between bottom and top heavy IMFs.
- The strong dependence of the PISN rate on the shape of the Pop III IMF and how it is populated means the details of modeling of PISN rates must be a critical component of successfully extrapolating the underlying astrophysics of the first stars from observed PISN rates. Specifically, we find populating the Pop III IMF with a Monte Carlo approach produces PISN rates which an order of magnitude lower with greater dependence on the IMF than their statistical counterparts. Therefore, the interpretation of observed PISN rates is strongly dependent on how the Pop III IMF is populated in the models.

As previously mentioned, the recent analysis of SN2018ibb as a potential PISN (Schulze et al. 2023) highlights the complexities of PISN rate predictions. With $M_{\text{peak}} \approx -21.8$, SN2018ibb would be detectable to $z \sim 10$, with a duration of 50-100 days. A more complex analysis which incorporates a variable PISN duration in the context of planned PISN surveys with JWST and Roman will be the subject of future study.

The authors acknowledge the University of Maryland supercomputing resources (<http://hpcc.umd.edu>) made available for conducting the research reported in this paper.

REFERENCES

- Abel T., Bryan G. L., Norman M. L., 2000, *ApJ*, 540, 39
- Abel T., Bryan G. L., Norman M. L., 2002, *Science*, 295, 93
- Barkat Z., Rakavy G., Sack N., 1967, *Phys. Rev. Lett.*, 18, 379
- Behroozi P. S., Wechsler R. H., Wu H.-Y., Busha M. T., Klypin A. A., Primack J. R., 2013, *ApJ*, 763, 18
- Bennett C. L., et al., 2013, *ApJS*, 208, 20
- Bovill M. S., Stiavelli M., Wiggins A. I., Ricotti M., Trenti M., 2024, *ApJ*, 962, 49
- Briel M. M., Eldridge J. J., Stanway E. R., Stevance H. F., Chrimes A. A., 2022, *MNRAS*, 514, 1315
- Bromm V., Coppi P. S., Larson R. B., 1999, *ApJ*, 527, L5
- Clark P. C., Glover S. C. O., Klessen R. S., Bromm V., 2011, *ApJ*, 727, 110
- Diego J. M., Broadhurst T., Zitrin A., Lam D., Lim J., Ford H. C., Zheng W., 2015, *MNRAS*, 451, 3920
- Diego J. M., Broadhurst T., Wong J., Silk J., Lim J., Zheng W., Lam D., Ford H., 2016, *MNRAS*, 459, 3447
- Fowler W. A., Hoyle F., 1964, *ApJS*, 9, 201
- Gal-Yam A., et al., 2009, *Nature*, 462, 624
- Gardner J. P., et al., 2006, *Space Sci. Rev.*, 123, 485
- Gill S. P. D., Knebe A., Gibson B. K., 2004, *MNRAS*, 351, 399
- Greif T. H., Springel V., White S. D. M., Glover S. C. O., Clark P. C., Smith R. J., Klessen R. S., Bromm V., 2011, *ApJ*, 737, 75
- Hahn O., Abel T., 2011, *MNRAS*, 415, 2101
- Heger A., Woosley S. E., 2010, *ApJ*, 724, 341
- Heger A., Fryer C. L., Woosley S. E., Langer N., Hartmann D. H., 2003, *ApJ*, 591, 288
- Jaacks J., Thompson R., Finkelstein S. L., Bromm V., 2018, *MNRAS*, 475, 4396
- Jauzac M., et al., 2015a, *MNRAS*, 446, 4132
- Jauzac M., et al., 2015b, *MNRAS*, 452, 1437
- Knollmann S. R., Knebe A., 2009, *ApJS*, 182, 608
- Lam D., Broadhurst T., Diego J. M., Lim J., Coe D., Ford H. C., Zheng W., 2014, *ApJ*, 797, 98
- Latif M. A., Whalen D., Khochfar S., 2022, *ApJ*, 925, 28
- Lazar A., Bromm V., 2022, *MNRAS*, 511, 2505
- Moriya T. J., Quimby R. M., Robertson B. E., 2022, *ApJ*, 925, 211
- Ohkubo T., Nomoto K., Umeda H., Yoshida N., Tsuruta S., 2009, *ApJ*, 706, 1184
- Park J., Ricotti M., Sugimura K., 2021a, *MNRAS*, 508, 6176
- Park J., Ricotti M., Sugimura K., 2021b, *MNRAS*, 508, 6193
- Prole L. R., Clark P. C., Klessen R. S., Glover S. C. O., 2022, *MNRAS*, 510, 4019
- Rakavy G., Shaviv G., Zinamon Z., 1967, *ApJ*, 150, 131
- Rieke G. H., et al., 2008, *AJ*, 135, 2245
- Rose B. M., et al., 2021, arXiv e-prints, p. arXiv:2111.03081
- Rydberg C.-E., Zackrisson E., Lundqvist P., Scott P., 2013, *MNRAS*, 429, 3658
- Salpeter E. E., 1955, *ApJ*, 121, 161
- Schulze S., et al., 2023, arXiv e-prints, p. arXiv:2305.05796
- Skinner D., Wise J. H., 2020, *MNRAS*, 492, 4386
- Springel V., 2005, *MNRAS*, 364, 1105
- Stacy A., Bromm V., Lee A. T., 2016, *MNRAS*, 462, 1307
- Stiavelli M., 2009, From First Light to Reionization: The End of the Dark Ages
- Sugimura K., Matsumoto T., Hosokawa T., Hirano S., Omukai K., 2020, *ApJ*, 892, L14
- Susa H., 2013, *ApJ*, 773, 185
- Susa H., Hasegawa K., Tominaga N., 2014, *ApJ*, 792, 32
- Vanzella E., et al., 2020, *MNRAS*, 494, L81
- Venditti A., Bromm V., Finkelstein S. L., Graziani L., Schneider R., 2024, *MNRAS*, 527, 5102
- Wang L., et al., 2017, arXiv e-prints, p. arXiv:1710.07005
- Weinmann S. M., Lilly S. J., 2005, *ApJ*, 624, 526
- Welch B., et al., 2022, *Nature*, 603, 815
- Whalen D. J., Fryer C. L., Holz D. E., Heger A., Woosley S. E., Stiavelli M., Even W., Frey L. H., 2013, *ApJ*, 762, L6
- Windhorst R. A., et al., 2018, *ApJS*, 234, 41
- Wollenberg K. M. J., Glover S. C. O., Clark P. C., Klessen R. S., 2020, *MNRAS*, 494, 1871
- Yoshida N., Omukai K., Hernquist L., Abel T., 2006, *ApJ*, 652, 6
- Zackrisson E., González J., Eriksson S., Asadi S., Safranek-Shrader C., Trenti M., Inoue A. K., 2015, *MNRAS*, 449, 3057